IEEE Access
Multidisciplinary | Rapid Review | Open Access Journal

Received 25 July 2024, accepted 17 August 2024, date of publication 23 August 2024, date of current version 2 September 2024.

Digital Object Identifier 10.1109/ACCESS.2024.3447890

RESEARCH ARTICLE

Low Frequency Gain Enhancement of Cavity-Backed Electrically-Small Hybrid Spiral Antenna for High-Voltage Partial Discharge Sensing

KRISTIAN CHAVDAROV DIMITROV[1], YONGSHIK LEE[1], (Senior Member, IEEE), JAE-HO YOUN[2], CHAN-UK PARK[2], SEUNG WON OH[2], AND MYOUNG-SOO LEE[2]

[1]Department of Electrical and Electronic Engineering, Yonsei University, Seoul 03722, South Korea
[2]GABO Corporation Ltd., Ansan-si, Gyeonggi-do 15617, South Korea

Corresponding author: Yongshik Lee (yongshik.lee@yonsei.ac.kr)

This work was supported by GABO Corporation Ltd.

ABSTRACT In this study, we propose a sensor for partial discharge (PD) sensing based on an electrically small hybrid spiral antenna, measuring approximately 0.087 wavelengths in diameter at 200 MHz. The sensor utilizes a hybrid design that integrates equiangular and Archimedes spiral antennas. Spiral antennas encounter significant gain loss when the wavelength exceeds their circumference, limiting their low-frequency performance. This can impede the early detection of PD, as the initial electromagnetic (EM) PD signature is concentrated at the low-frequency end of the ultrahigh frequency (UHF) band. In addition, PD sensors are often enclosed within a metallic cavity to shield them from surrounding noise. However, this further exacerbates the challenges of low-frequency performance, with the band of interest potentially falling well below the cavity cutoff frequency. In this study, we alleviate this limitation by integrating a capacitively loaded ring resonator with the spiral antenna, thereby enhancing its low-frequency gain without increasing the antenna size. Experimental results from a prototype sensor with an aperture diameter of 130 mm demonstrate that the proposed ring resonator increases the realized gain in a relatively wide bandwidth from 220 MHz to 650 MHz by as much as 18.3 dB, with minimal impact observed at higher frequencies. Moreover, in situ PD detection test results demonstrate an improvement of 0.6 dB in the mean received power, along with a spectral efficiency improvement in the frequency range of 290-525 MHz, with a peak improvement of 21.2 dB in the received power spectral density (PSD) at 410 MHz.

INDEX TERMS Cavity antenna, electrically small, partial discharge, sensor, UHF antenna, wideband antenna.

I. INTRODUCTION

Partial discharge (PD) [1], [2], [3] is a transient phenomenon occurring in high-voltage systems, characterized by localized insulation breakdown between two conductors. Early detection and diagnosis are crucial for preventing significant damage to equipment and/or endangerment of personnel. Partial discharge events emit acoustic, optical, and chemical signatures [4], [5]. Additionally, a fast transient current pulse occurs, leading to wideband electromagnetic (EM) radiation, which is the focus of this work. Depending on the insulation breakdown stage, both the strength and spectral content of the radiated EM emissions evolve over time [6]. For example, although the majority of radiation falls within a wide frequency range of hundreds of MHz to a few GHz [7], corresponding to the ultrahigh frequency (UHF)

The associate editor coordinating the review of this manuscript and approving it for publication was Santi C. Pavone.

band, the radiation emitted when initial insulation failure occurs, is relatively weak and predominantly concentrated in the lower end of the frequency band. Thus, for the early diagnosis of insulation failure, both high sensitivity and robust low-frequency performance are crucial for PD sensors.

Various UHF antenna-based PD sensors have been proposed [8], [9], [10], [11], [12]. Among them, spiral antennas have been a popular choice [10], [11], [12], due to their frequency-independent characteristics and circular polarization. However, the effectiveness of these antennas, not unlike others, is inherently limited at frequencies at which the antenna is electrically small. In spiral antennas, radiation arises only in the active region, which occurs when the circumference of the curved pattern is one wavelength [13]. Thus, the lowest frequency of operation is determined by the circumference of the antenna. Below this frequency, the active region no longer exists, owing to the finite size of the antenna. Consequently, the antenna can no longer radiate efficiently, and both a rapid increase in the input reflection and a corresponding decline in gain are inevitable [14], [15].

Efforts to enhance the effectiveness of PD sensors using spiral antennas have successfully refined their characteristics [10], [11], [12]. However, these improvements were mostly accomplished at frequencies at which the antenna is electrically large. For example, in [10], a method is demonstrated to suppress a parasitic resonance of a cavity-backed spiral antenna caused by unusually large cavity backing. The method effectively compensates for the degraded gain by 21 dB, from 6 dBic to −15 dBic, at 1.3 GHz at which the antenna measures 1.21 wavelengths (λ_0) in diameter. However, this alteration tends to decrease the gain of the antenna at low frequencies, as it is primarily focused on the frequencies around the cavity resonance. Similarly, in [11], the enhancement of the reflection characteristics of a dual-arm cosine slot spiral antenna was limited to the band in which the antenna size is sufficiently large, specifically between 1 and 2.25 wavelengths (λ_0). One straightforward approach to improve the gain at low-frequencies is to lower its operational frequency by increasing the antenna size. However, deploying larger antennas may not always be practical or compatible with the installation requirements of PD sensors.

Partial discharge sensors are typically backed with a metallic cavity to minimize the effect of surrounding noise and preserve shielding integrity. The cavities must be compatible with the standard mounting flanges used in high-voltage equipment. This imposes further restrictions on the antenna size, and thus, limits its lower operational frequency. In addition, the metallic cavity exacerbates the problem with the low-frequency gain, due of its adverse effect on the gain and reflection coefficient of the antenna, as the frequency band of interest can extend considerably bellow the cutoff frequency of the cavity.

In this work, we present a method to enhance the low-frequency realized gain of PD sensors based on a cavity-backed spiral antenna by integrating a reactively loaded ring resonator with the spiral antenna. This is performed at low frequencies, which are normally considered below the standard operational range of the antenna. The ring resonator is utilized to introduce an additional resonance near the lowest operational frequency of the spiral antenna, enabling significant improvement in the low-frequency gain without adversely affecting the high-frequency performance and, most importantly, without increasing the size of the sensor.

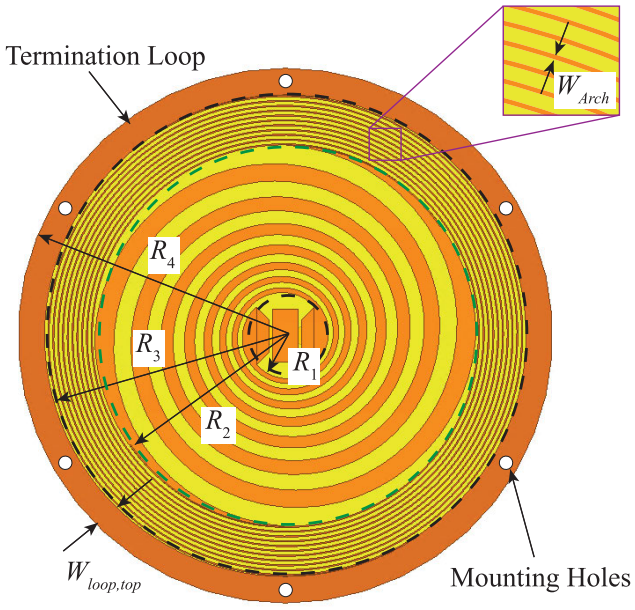

FIGURE 1. Layout of hybrid antenna consisting of equiangular spiral ($R_1 \le r \le R_2$), Archimedes spiral ($R_2 \le r \le R_3$) and termination loop.

The proposed method is validated with experimental results obtained from a prototype sensor designed with a diameter of 130 mm, which is 0.087 wavelengths at 200 MHz. The realized gain increased within the 220-650 MHz range, with the measured peak gain improvement reaching 18.3 dB at 320 MHz. In situ test of the sensor's ability to receive PD emissions also demonstrated improved detection sensitivity and spectral efficiency. The mean received power is increased by 0.6 dB, and peak spectral efficiency improvement of 21.2 dB is achieved, validating the proposed method to enhance the low-frequency realized gain and sensitivity of PD sensors based on spiral antennas.

II. SENSOR DESIGN

The proposed sensor consists of a hybrid spiral antenna [16], [17] between an equiangular spiral [13] and an Archimedes spiral [18], and a termination loop, as illustrated in Fig. 1. In this study, the orientation of both spirals is such that the sensor has right-handed circular polarization (RHCP). The equiangular spiral is positioned on the inner side of the entire sensor structure between R_1 and R_2, facilitating efficient

radiation at high frequencies. Conversely, the Archimedes spiral is located on the outer side between R_2 and R_3, terminating in the loop, and ensuring efficient radiation at lower frequencies.

The Archimedes spiral has a constant rate of growth and can be expressed via the function in (1a) in polar coordinates [18].

$$R(\phi) = R_{min} + A\phi, \tag{1a}$$
$$A = (R_{max} - R_{min})/2\pi N_{Arch}. \tag{1b}$$

The antenna can be defined using its minor radius $R_{min} = R_2$, growth constant A, and angle variable ϕ. The growth constant A can also be expressed as a function of the major radius of the antenna $R_{max} = R_3$ and the number of turns N_{Arch}, as in (1b), where $2\pi N$ is the maximum value of the argument ϕ. Similarly, an equiangular spiral, with minor and major radii of $R_{min} = R_1$ and $R_{max} = R_2$, can be constructed from two radii functions R_a and R_b, defined by (2a) and (2b) [13] respectively.

$$R_a(\phi) = R_{min} \times e^{A\phi}, \tag{2a}$$
$$R_b(\phi) = K \times R_{min} \times e^{A\phi}, \tag{2b}$$
$$A = \ln(R_{max}/R_{min})/2\pi N_{Log}, \tag{2c}$$
$$K = e^{A\delta}, \tag{2d}$$

where R_b is identical to R_a but rotated around the center axis determined by the coefficient δ in (2d), and N_{Log} is the number of turns.

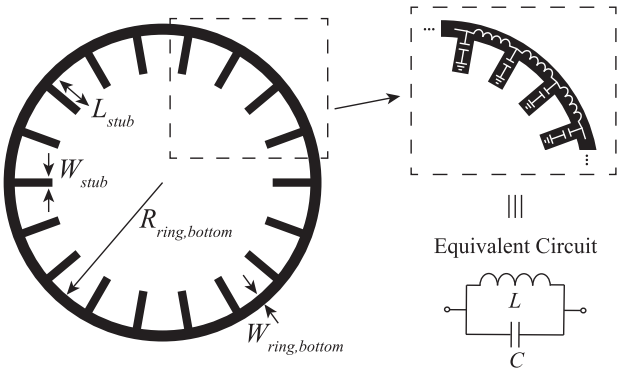

FIGURE 2. Ring resonator consisting of a ring, periodically loaded with capacitive stubs.

In this work, the capacitively loaded ring resonator shown in Fig. 2 is introduced underneath the spiral antenna to improve its low-frequency gain and sensitivity. Typically, a ring resonates at the frequency at which it has a circumference of one wavelength. To lower its resonant frequency, the ring resonator is periodically loaded with capacitive stubs, forming a distributed LC tank circuit. This adds an additional resonant frequency $f_{c,Ring} = 1/(2\pi\sqrt{L \times C})$, to the reflection coefficient characteristic of the antenna, whose position can be controlled not only by the radius $R_{ring,bottom}$ and width $W_{ring,bottom}$ of the ring, but also by the

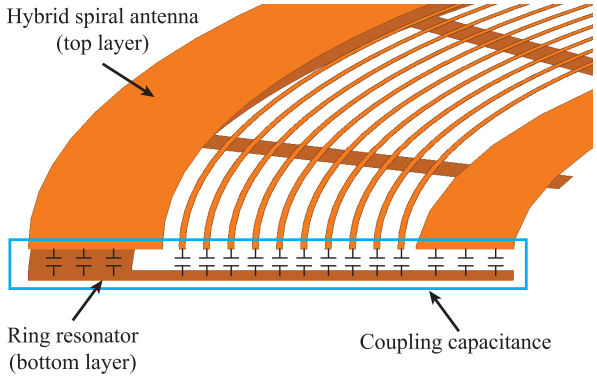

FIGURE 3. Spiral antennas coupled capacitively with ring resonator.

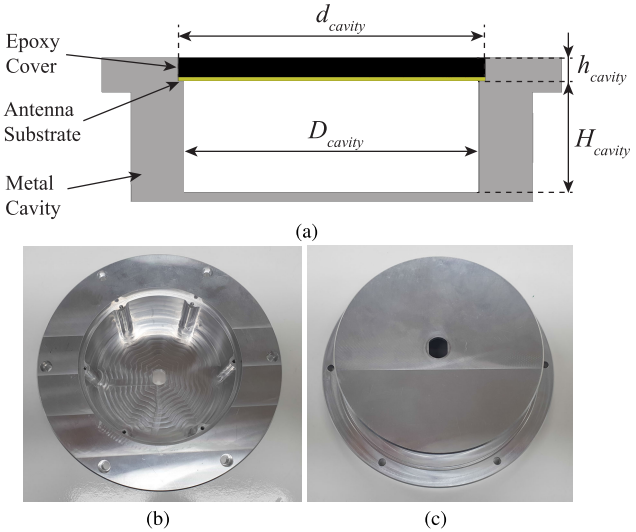

FIGURE 4. Aluminium cavity. (a) Cross section with dimensions. Cavity photographs of (b) top and (c) bottom view. (D_{cavity} = 126 mm, d_{cavity} = 131 mm, H_{cavity} = 47 mm, h_{cavity} = 10 mm.)

number of stubs N_{stub}, their width W_{stub} and length L_{stub}. These parameters can be determined such that the resonant frequency of the ring resonator $f_{c,Ring}$ is lower than the lowest operational frequency of the spiral antenna.

A crucial design consideration is the coupling capacitance between the turns of the Archimedes spiral antenna and ring resonator, as shown in Fig. 3. There should be a sufficient number of tightly wound spiral turns to promote a uniform field in the overlap region with the stubs of the ring resonator. This ensures that the coupling between the two is strong enough to excite the proposed ring resonator efficiently. Otherwise, the impact of the additional resonance on the realized gain of the antenna may be negligible.

Based on these considerations, a prototype sensor was designed. The design objective was to maintain the equiangular spiral as the dominant part, maximizing its size to achieve high efficiency at higher frequencies. The optimization of the Archimedes spiral is also crucial, not only for low-frequency operation, but also for facilitating coupling with the proposed

TABLE 1. Summary of all design parameters.

Dimension	Value	Dimension	Value
R_1	10.0 mm	N_{Arch}	5
R_2	46.6 mm	N_{Log}	3.75
R_3	59.0 mm	N_{stub}	18
R_4	65.0 mm	δ	1.53
W_{Arch}	0.3 mm	$R_{ring,bottom}$	60.5 mm
$W_{loop,top}$	6.0 mm	$W_{ring,bottom}$	4.5 mm
L_{stub}	18.5 mm	W_{stub}	3.0 mm
H_{cavity}	47.0 mm	D_{cavity}	126.0 mm
h_{cavity}	10.0 mm	d_{cavity}	131.0 mm
h_{ant}	1.6 mm		

ring resonator, which is essential for gain improvement at lower frequencies.

The antenna is designed on a substrate with a permitivity of 4.4 and a height of $h_{ant} = 1.6$ mm. It has outer radius of $R_4 = 65$ mm, and internal of $R_1 = 10.0$ mm, $R_2 = 46.5$ mm and $R_3 = 59.0$ mm. The equiangular spiral operates efficiently as a circularly polarized radiator down to its minimum operational frequency $f_{min,Log} = c/(2\pi R_2) = 1027$ MHz, determined by its circumference. Similarly, the Archimedes spiral operates down to $f_{min,Arch} = c/(2\pi R_3) = 809$ MHz. Below these frequencies, not only the gain and input matching deteriorate rapidly, but also the antenna becomes linearly polarized [13]. To mitigate the decrease in gain below $f_{min,Arch}$, the parameters of the ring resonator are optimized to introduce an additional resonance at a frequency lower than these thresholds.

Additionally, the cavity backing of the antenna with a diameter of $D_{cavity} = 126$ mm and depth of $H_{cavity} = 47$ mm, which has a cutoff of 697 MHz, is depicted in Fig. 4. The antenna was positioned within a recess measuring $d_{cavity} = 131$ mm in diameter, $h_{cavity} = 10$ mm below the cavity surface. This recess allows for the placement of an epoxy superstrate with thickness of 8.40 mm, nominal dielectric permittivity of 4.4 and loss tangent of 0.02 to provide mechanical protection for the antenna. A summary of all relevant antenna and cavity dimensions is provided in Table 1.

Fig. 5 compares the simulated performance of the proposed and conventional sensors, where both are identical, except that the former incorporates the proposed ring resonator. The simulation model used to acquire the data shown in Fig. 5 uses ideal lossless feeding to obtain the unadulterated performance of the sensors. In Section III-B, simulated and measured results using practical feeding with a balun are provided. All simulation results presented in this work were obtained using the ANSYS HFSS EM simulator package [19]. The reflection coefficient, shown in Fig. 5(a), for both sensors remains below −10 dB for most of the band below 600 MHz, it increases to approximately −5 dB below 550 MHz. However, notably an additional resonance was introduced in the proposed sensor by the integrated ring resonator at $f_{c,Ring} = 380$ MHz.

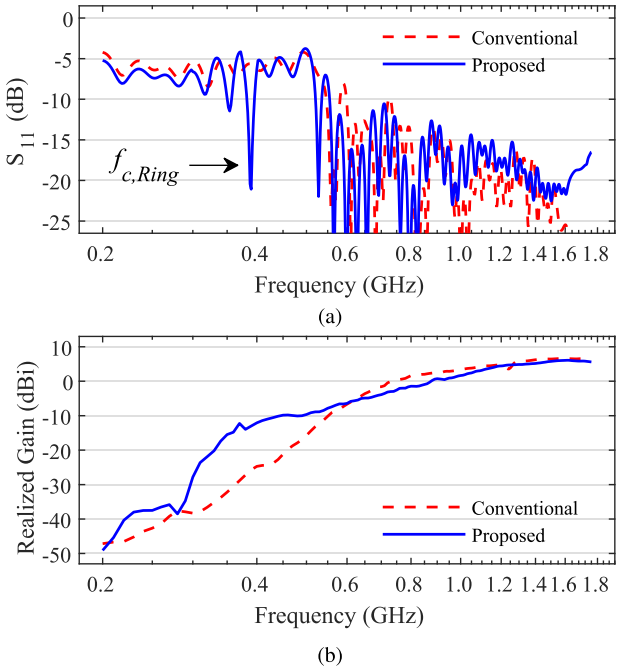

FIGURE 5. Simulated (a) input reflection coefficient and (b) boresight total realized gain of the conventional and proposed sensors, using ideal feeding without a balun.

Similar to other antennas, the gain of the conventional sensor deteriorates as the frequency decreases. This can be observed in Fig. 5(b), where the gain decreases rapidly below $f_{min,Arch}$, when the diameter becomes approximately a wavelength. At $f_{min,Arch}$ the simulated total gain measures 1.6 dBi and reaches as low as −38.3 dBi at 300 MHz. The results in Fig. 5(a) show that the improvement in input matching due to the ring resonator occurs over a relatively narrow bandwidth, whereas its impact on the gain is observed over a much broader range. A comparison of the gains in Fig. 5(b)) reveals that the gain improvement due to the additional resonance is achieved over a considerable 2.75:1 bandwidth between 220 and 605 MHz, with more than a 3 dB increase between 223 and 533 MHz.

III. FABRICATION AND MEASUREMENT

A. PD SENSOR FABRICATION

Using standard printed circuit board (PCB) fabrication technology, the designed sensor was fabricated on a $h_{ant} = 1.6$ mm thick FR-4 epoxy laminate substrate with 35 µm copper foil and a PCB diameter of $2 \times R_4 = 130$ mm. The spiral antennas are patterned on the top layer of the PCB, whereas the ring resonator along with the feeding circuit are on the bottom layer. The PCB was then placed within the metallic cavity, as shown in Fig. 4, with the spiral pattern facing outward, and fastened using metallic screws. The soldermask along the edge of the PCB's bottom layer is omitted, allowing the PCB to make contact with the cavity along its perimeter, connecting the cavity and the ring

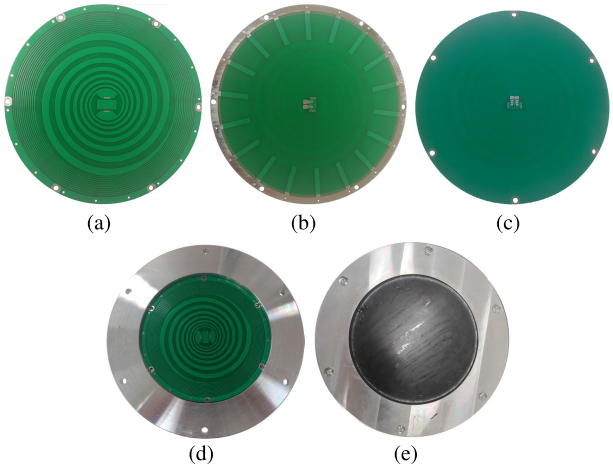

FIGURE 6. Images of the fabricated sensor. Antenna PCB (a) top view, bottom view of the (b) proposed and (c) conventional sensors. (d) the PCB mounted within the metal cavity and (e) the sensor with an epoxy superstrate.

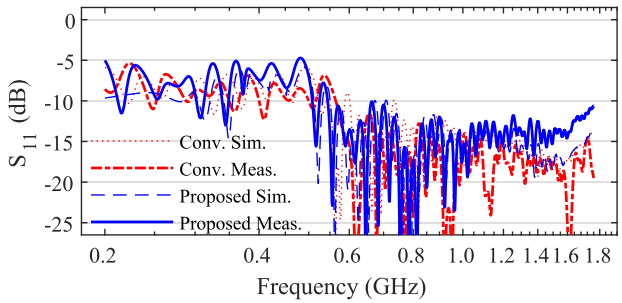

FIGURE 7. Comparison of input reflection coefficient of complete sensor including balun and feeding cable.

resonator electrically. The mounting screws and 18 plated via holes (Fig. 6(a)) were placed along the perimeter of the antenna to connect the ring resonator and termination loop. The sensor is fed via a bulkhead mount N-connector at the bottom side of the cavity, which is connected to the PCB using a 70 mm of 0.047″ semi-rigid coaxial cable. Spiral antennas are balanced structures and thus must be excited with a balun [13]. A transformer balun [20] is utilized in this work due to space limitations, despite its higher loss compared to a tapered line balun, as that used in [10]. In the fabricated antennas, a commercial transformer-type balun TCM2-33X+ [21] with an impedance ratio of 2:1 and nominal insertion loss of 1.5 dB is used between the input of the antenna and the feeding coaxial cable providing impedance matching and balanced output. Photographs of the sensors before and after assembly are shown in Fig. 6.

B. RADIATION PARAMETERS MEASUREMENT

First, the electromagnetic performance of the sensors was measured. The input reflection coefficient was measured from 200 MHz to 1.8 GHz using a vector network analyzer (VNA) MS46122B from Anritsu, which was calibrated using an SOLT (short open load thru) calibration kit TOSLKF50A. The measured results for both the proposed and conventional sensors are compared with the simulated, as shown in Fig. 7. Both sensors exhibit a similar reflection coefficient performance, maintaining below −5 dB up to approximately 600 MHz, which then improves to below −10 dB. The resonant peak of the ring resonator, as obtained from the simulated results in Fig. 5(a), is no longer visible because it is masked by the additional insertion and return loss of the balun.

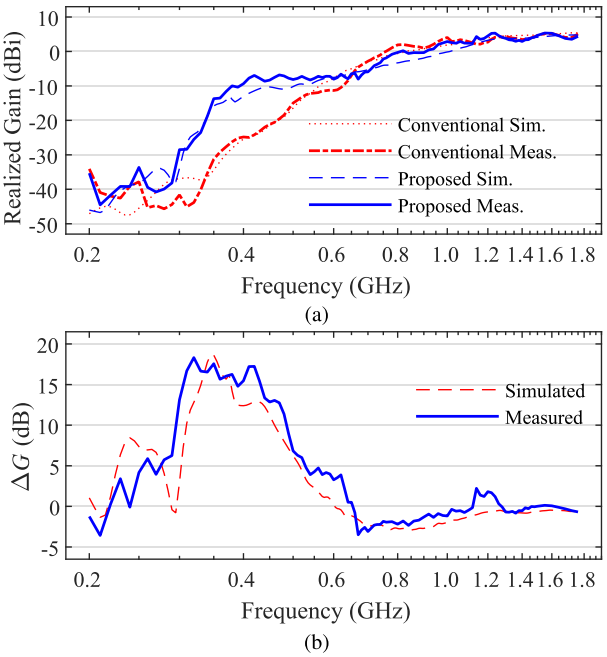

FIGURE 8. (a) Comparison of boresight total realized gain of completed sensors including balun. (b) Gain improvement due to proposed ring resonator.

The radiation pattern and gain were measured in a tapered anechoic chamber using an Agilent Technologies VNA E8364B. The measured realized gain exhibits good agreement with the simulated across the majority of the band, as shown in Fig. 8(a). The maximum total realized gain is 5.22 dBi at 1.55 GHz and 5.35 dBi at 1.77 GHz for the proposed and conventional sensors respectively. The influence of the ring resonator is minimal at higher frequencies, as evidenced by the closely matched gains of the two sensors. However, a notable enhancement in gain is discernible at lower frequencies.

Fig. 8(b) illustrates the gain improvement, obtained from 220 MHz to 650 MHz and surpassing 3 dB between 229 MHz and 625 MHz, with the peak improvement reaching 18.3 dB at 320 MHz. This underscores the compelling evidence of the ring resonator's efficacy in fortifying the performance of the sensor, especially at lower frequencies, which is crucial for PD sensing applications. For example, for a conventional spiral antenna, without the proposed ring resonator, to achieve similar gain as the

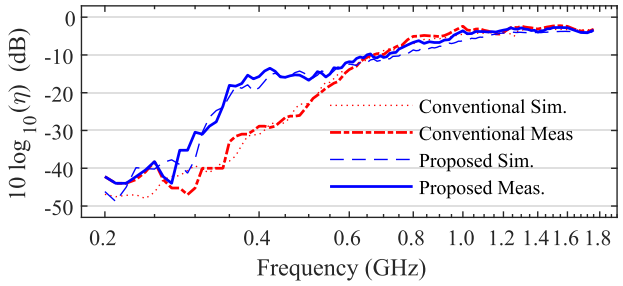

FIGURE 9. Total efficiency of the conventional and proposed sensors.

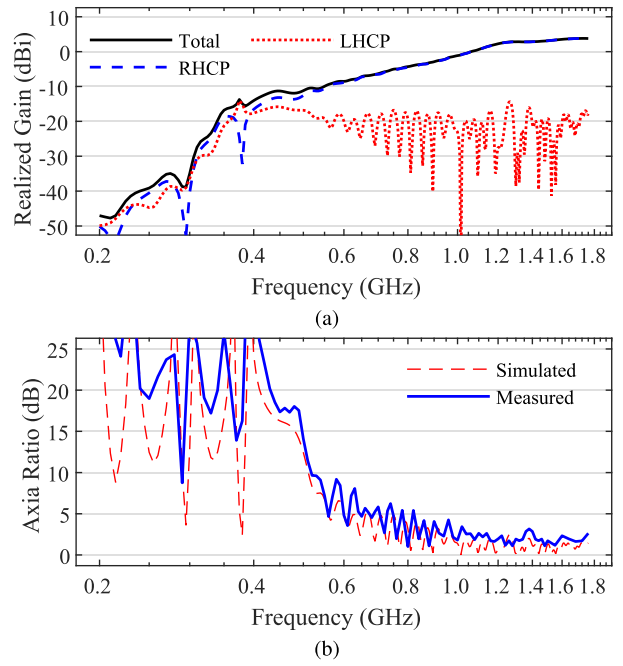

FIGURE 10. (a) Simulated total, right- and left- handed circular polarization realized gain components in boresight direction, and (b) axial ratio of the proposed sensor.

proposed antenna at the ring resonator's resonant frequency $f_{c,Ring} = 380$ MHz, the size of the radiation element must be increased from $R_3 = 59$ mm to $R_3 = 97$ mm. This corresponds to an increase of more than 170 % in area.

The total efficiency η of the antenna is shown in Fig. 9, where the measured efficiency closely matches the simulated. A comparison between the efficiencies of the proposed and conventional sensors reveals that the ring resonator increases the efficiency at low frequencies, whereas the efficiencies at high frequencies remain virtually intact. This leads to a substantial improvement in the realized gain at lower frequencies and, enhancing the sensitivity and making the proposed method much more suitable for PD detection. Moreover, the efficiency above $f_{min,Arch}$, where the antenna exhibits a good impedance match, is approximately -3 dB, as shown in Fig. 7. This value corresponds to the insertion loss of the sensor, which is mostly due to the loss of the epoxy superstrate and the balun.

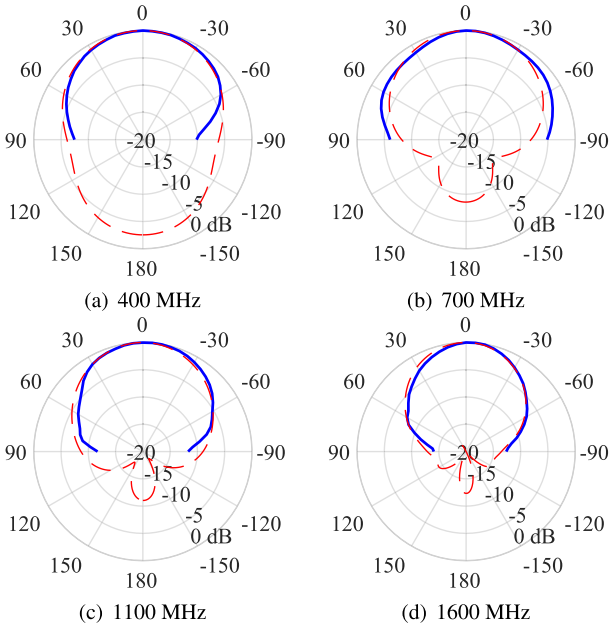

FIGURE 11. Normalized radiation patterns azimuth cut of the proposed sensor (solid: measured, dashed: simulated).

As previously noted, one of the significant advantages of spiral-antenna based sensors is their insensitivity to polarization. This characteristic is particularly advantageous considering the polarization uncertainty of the PD emissions. The simulated partial realized gain polarization components of the proposed sensor are shown in Fig. 10(a). The results show that the sensor exhibits good RHCP behavior, particularly above 809 MHz, which is the lowest operational frequency of the spiral. Below this frequency, the sensor tends towards linear polarization, and its polarization angle changes rapidly with frequency. This change in the polarization properties with respect to frequency is a common characteristic of spiral antennas operating below their designed frequency [13], and is clearly visible in the axial ratio shown in Fig. 10(b). Some discrepancy between the simulated and measured axial ratio can be observed at frequencies below 500 MHz. This is partly because of the low number of measurement points. Additionally, as discussed above, the antenna becomes linearly polarized in this frequency range. This implies that the magnitude of the electric field along the major axis of the polarization ellipse is significantly larger than that along the minor axis. As the axial ratio is the ratio of these two, a small measurement error may result in a significantly large difference.

The radiation patterns of the proposed sensor at various frequencies are shown in Fig. 11. Regardless of the frequency, the measured agrees greatly with the simulated, with the maximum gain in the broadside direction. Notably, owing to the inherent symmetry of the sensor's structure, the pattern also exhibits rotational symmetry.

The sensitivity of a PD sensor can be judged by its effective height h_e metric [22], [23], [24]. The h_e is defined as the

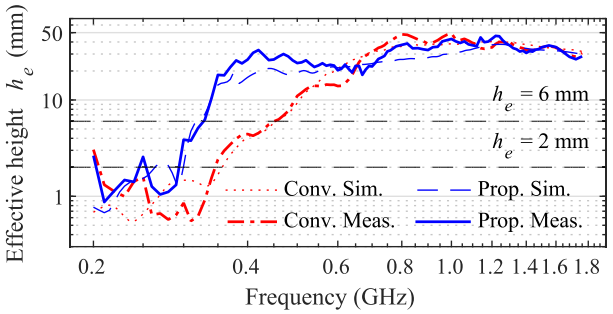

FIGURE 12. Effective height h_e of the sensors.

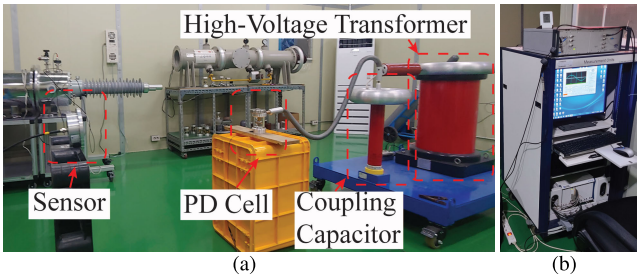

FIGURE 13. (a) Partial discharge measurement setup. (b) Partial discharge strength detection system and controller.

inverse of the antenna factor AF, which is the ratio between the open circuit voltage at the input of the sensor V_o and the incident electric field strength E_i inducing it. The effective height can be calculated using (3)

$$h_e = \frac{1}{AF} = \frac{|V_o|}{|E_i|}, \tag{3}$$

and has units of meters. The calculated h_e are shown in Fig. 12. The effective height of the conventional sensor remains above the 2 mm and 6 mm thresholds down to 345 MHz and 460 MHz respectively. The corresponding values of the proposed sensor are 295 MHz and 330 MHz, improving the 2 mm and 6 mm threshold frequency values by a factor of 1.17 and 1.39.

C. PARTIAL DISCHARGE DETECTION MEASUREMENT

For experimental verification of improved sensitivity, due to the enhanced sensor's gain, both the conventional and proposed sensors underwent testing for PD detection. A PD cell was used to consistently simulate the radiation emissions from a failure, which were measured using both sensors. The experiment was conducted within a shielded chamber to mitigate the influence of external noise sources on the measurements. The test setup, illustrated in Fig. 13, comprised of an oil-filled PD cell of particle type [25], [26], a high-voltage transformer, a coupling capacitor, and a PD control and monitoring system. The sensors were positioned 1 m away from the PD cell on a non-metallic surface approximately 1 m above the chamber's floor. Partial discharge was induced with a peak charge of 100 nC, excited

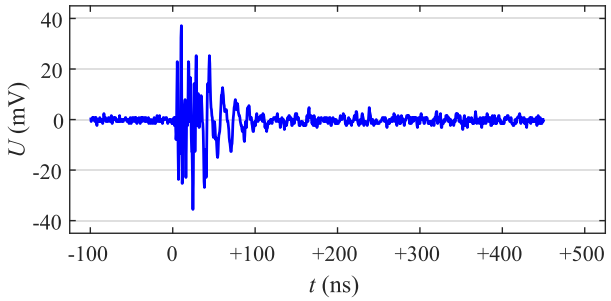

FIGURE 14. An example of measured time resolved PD pulse.

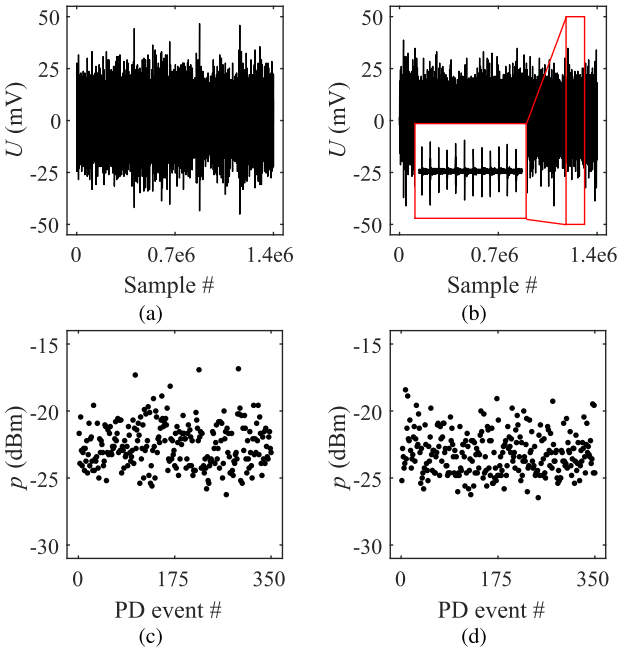

FIGURE 15. Captured 350 PD pulses with (a) proposed and (b) conventional sensors in the time domain, with the dead time between pulses removed. Calculated peak received power measured with the (c) proposed and (d) conventional sensors.

by a 60 Hz 11.9 kV voltage signal. The EM emissions from the PD cell were captured in the time domain using a high-speed oscilloscope RTO2044 from Rohde & Schwarz, with an analog bandwidth of 4 GHz and a sampling rate of 20 GSa/s.

The phenomena of PD is an inherently stochastic process with a high degree of uncertainty, which produces large variations in the radiated power [27], [28]. In conjunction with environmental factors, such as multiple reflections, the received power level can vary significantly. Thus, to compare the performance of the two sensors, the probability distribution functions (PDF) of the received instantaneous power levels are required. To do so, a total of 350 PD events were measured over a span of 3 s. The duration of a PD pulse lasted approximately 100 ns, as illustrated in Fig. 14. The pulse repetition rate is 120 Hz, which is twice the frequency of the excitation voltage. This leads to approximately 8.3 ms of

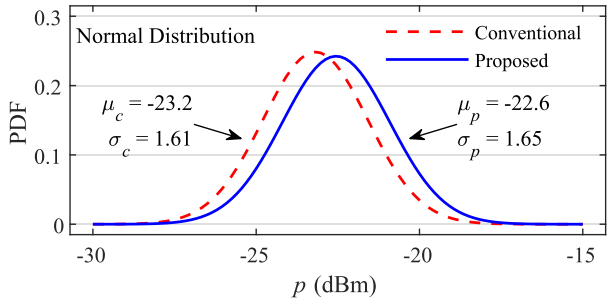

FIGURE 16. PDF of received peak instantaneous power.

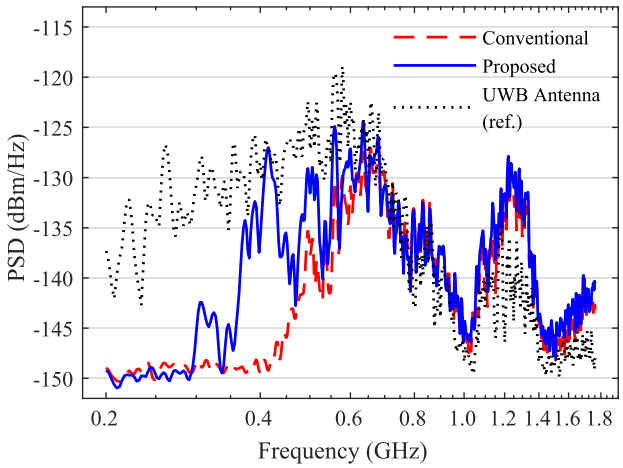

FIGURE 17. Received power spectral density PSD.

idle time between the pulses. Using the segmented memory function of the oscilloscope, the 350 PD events were captured with the dead time between events eliminated, as shown in Fig. 15(a) and 15(b).

For each event, the peak instantaneous power was calculated using (4).

$$p\,(\text{dBm}) = 30 + 10\log_{10}\left\{\left(\frac{V_{pp}}{2\sqrt{2}}\right)^2 \cdot \frac{1}{50}\right\}, \qquad (4)$$

where V_{pp} is the peak-to-peak measured voltage U in volts and 50 Ω is the input impedance of the oscilloscope. The calculated values are shown in Fig. 15(c) and 15(d). The probability distribution functions of the received instantaneous power levels were constructed by assuming a normal distribution, as shown in Fig. 16. As evidenced by the obtained PDFs, there is a clear distinction between the two, implying that the proposed sensor has a higher proclivity to induce an increase in the received power due to the increased gain resulting from the introduced ring resonator. The PDF of the conventional sensor has a mean value of $\mu_c = -23.2$ dBm and a deviation of $\sigma_c = 1.61$. The integration of the ring resonator shifts the curve to a mean value of $\mu_p = -22.6$ dBm and a deviation $\sigma_p = 1.65$. The results indicate that for the proposed structure, the mean received power has been increased by 0.6 dB, with a negligible difference in the deviation.

Finally, the received PD time domain signals were evaluated in the frequency domain. Due to the presence of noise, the captured data were averaged using Welch's method for power spectral density (PSD) estimation [29]. The analysis was performed with the data divided into 50 windows with 50% overlap, followed by a discrete Fourier transform with a length of 8193 points. The results are shown in Fig. 17. Whereas the high-frequency response remains practically the same, the spectra demonstrate a clear correlation between the obtained gain improvement (Fig. 8(b)) and the enhanced spectral efficiency at lower frequencies. The ring resonator increased the received PSD across the majority of the band between 290 MHz and 525 MHz, with a peak increase of 21.2 dB at 410 MHz.

Additionally, the radiation spectrum captured using a reference ultra-wideband (UWB) antenna with vertical polarization and gain of more than 0 dBi from 300 MHz is depicted in Fig. 17. It clearly shows that the EM signature of the PD events is concentrated at lower frequencies. Therefore, a gain improvement in this range will have a significant impact on the peak received power, highlighting the effectiveness of the proposed low-frequency enhancement technique in increasing the sensitivity of the sensor.

IV. CONCLUSION

In this study, we propose an approach to enhance the low-frequency sensitivity of cavity-backed electrically small spiral antennas used as UHF sensors for PD detection. For such antennas, performance degradation is inevitable as the wavelength surpasses the circumference of the antenna. Furthermore, these sensors are typically enclosed in a metallic cavity to minimize the effect of external noise and provide an uninterrupted shielding environment. This further exacerbates the circumstance, as for electrically small antennas, the cavity operates in cutoff mode at low frequencies. This potentially hinders the early diagnosis of PD, and therefore, the strong advantage of the polarization insensitivity of spiral antennas cannot be fully utilized. This is because the initial EM radiation emitted from the PD events is concentrated in the lower frequency range.

To fully leverage the versatility of spiral antennas as PD sensors, we integrated a planar capacitively-loaded ring resonator, coupled with a spiral antenna. This introduces an additional resonance that can be optimized to extend the low-frequency limit of the spiral antenna. This enhancement makes spiral antennas much more attractive for PD sensor applications, as their polarization advantage can be fully utilized. Experimental results for a sensor employing a hybrid design of equiangular and Archimedes spiral antennas, backed by a cylindrical metallic cavity, demonstrate that the ring resonator significantly increases the realized gain

towards the low-frequency end, ranging from 220 MHz to 650 MHz, whereas maintaining virtually intact high-frequency response. The improvement surpasses 3 dB between 229 MHz and 625 MHz, with the peak improvement reaching 18.3 dB at 320 MHz. Additionally, the effective height threshold frequencies of 2 mm and 6 mm were lowered by a factor of 1.17 and 1.39 respectively.

An in situ PD detection experiment encompassing 350 PD events was conducted. Results indicate a mean improvement of 0.6 dB in received power. Spectral performance, assessed by performing Welch PSD estimate on the recorded time-domain received data, reveals a clear correlation between improved gain and increased spectral density. The received PSD increased in the majority of the band between 290 MHz and 525 MHz, with a peak increase of 21.2 dB at 410 MHz. This validates the effectiveness of the proposed method for enhancing the sensitivity of PD sensors at low frequencies based on electrically small spiral antennas. Finally, the gain improvement bandwidth can be further expanded by integrating additional ring resonators and/or multi-mode resonators, albeit at the expense of increased structural and design complexity.

REFERENCES

[1] R. Bartnikas, "Partial discharges. Their mechanism, detection and measurement," *IEEE Trans. Dielectr. Elect. Insul.*, vol. 9, no. 5, pp. 763–808, Oct. 2002, doi: 10.1109/TDEI.2002.1038663.

[2] P. H. F. Morshuis and J. J. Smit, "Partial discharges at DC voltage: Their mechanism, detection and analysis," *IEEE Trans. Dielectr. Elect. Insul.*, vol. 12, no. 2, pp. 328–340, Apr. 2005, doi: 10.1109/TDEI.2005.1430401.

[3] N. H. Ahmed and N. N. Srinivas, "On-line partial discharge detection in cables," *IEEE Trans. Dielectr. Elect. Insul.*, vol. 5, no. 2, pp. 181–188, Apr. 1998, doi: 10.1109/94.671927.

[4] *IEEE Guide to the Measurement of Partial Discharge in Rotating Machinery*, New York, NY, USA, IEEE Standard 1434-2000, 2000.

[5] *High-Voltage Test Techniques—Partial Discharge Measurements*, IEC Standard 60270-2000, Geneva, Switzerland, 2000.

[6] F. Tian, X. Li, S. Zhang, and J. Cao, "The partial discharge evolution characteristics of 10kV XLPE cable joint," *IEEE Access*, vol. 11, pp. 108680–108687, 2023, doi: 10.1109/ACCESS.2023.3321805.

[7] S. Tenbohlen, D. Denissov, S. M. Hoek, and S. M. Markalous, "Partial discharge measurement in the ultra high frequency (UHF) range," *IEEE Trans. Dielectr. Elect. Insul.*, vol. 15, no. 6, pp. 1544–1552, Dec. 2008, doi: 10.1109/TDEI.2008.4712656.

[8] S. Kaneko, S. Okabe, M. Yoshimura, H. Muto, C. Nishida, and M. Kamei, "Detecting characteristics of various type antennas on partial discharge electromagnetic wave radiating through insulating spacer in gas insulated switchgear," *IEEE Trans. Dielectr. Electr. Insul.*, vol. 16, no. 5, pp. 1462–1472, Oct. 2009, doi: 10.1109/TDEI.2009.5293961.

[9] G. Robles, R. Albarracin, and J. L. Vazquez, "Antennas in partial discharge sensing system," in *Handbook of Antenna Technologies*, Z. Chen, Ed. Sigapore: Springer, 2015, doi: 10.1007/978-981-4560-75-7-95-1.

[10] S. Park and K.-Y. Jung, "Design of a circularly-polarized UHF antenna for partial discharge detection," *IEEE Access*, vol. 8, pp. 81644–81650, 2020, doi: 10.1109/ACCESS.2020.2991158.

[11] Y. R. Yadam, R. Sarathi, and K. Arunachalam, "Planar ultrawideband circularly polarized cosine slot Archimedean spiral antenna for partial discharge detection," *IEEE Access*, vol. 10, pp. 35701–35711, 2022, doi: 10.1109/ACCESS.2022.3163303.

[12] Y. R. Yadam, S. Ramanujam, and K. Arunachalam, "Study of polarization sensitivity of UHF sensor for partial discharge detection in gas insulated switchgear," *IEEE Sensors J.*, vol. 23, no. 2, pp. 1214–1223, Jan. 2023, doi: 10.1109/JSEN.2022.3224475.

[13] J. Dyson, "The equiangular spiral antenna," *IRE Trans. Antennas Propag.*, vol. 7, no. 2, pp. 181–187, Apr. 1959, doi: 10.1109/TAP.1959.1144653.

[14] R. Sammeta and D. S. Filipovic, "Quasi frequency-independent increased bandwidth planar log-periodic antenna," *IEEE Trans. Antennas Propag.*, vol. 62, no. 4, pp. 1937–1944, Apr. 2014, doi: 10.1109/TAP.2014.2302001.

[15] P. E. Mayes, "Frequency-independent antennas and broad-band derivatives thereof," *Proc. IEEE*, vol. 80, no. 1, pp. 103–112, Jan. 1992, doi: 10.1109/5.119570.

[16] C. Baard, Y. Liu, and N. Nikolova, "Ultra-wideband low-cost high-efficiency cavity-backed compound spiral antenna," *Electronics*, vol. 9, no. 9, p. 1399, Aug. 2020, doi: 10.3390/electronics9091399.

[17] D. Chen, H. Zhang, and J. Xu, "A broadband planar spiral antenna design for electromagnetic signal monitoring," *IEEE Access*, vol. 8, pp. 73451–73456, 2020, doi: 10.1109/ACCESS.2020.2971135.

[18] J. Kaiser, "The Archimedean two-wire spiral antenna," *IRE Trans. Antennas Propag.*, vol. 8, no. 3, pp. 312–323, May 1960, doi: 10.1109/TAP.1960.1144840.

[19] ANSYS. *ANSYS HFSS [Software]*. Canonsburg, PA, USA. Accessed: Apr. 22, 2024. [Online]. Available: https://www.ansys.com/products/electronics/ansys-hfss

[20] N. Nishizuka, M. Sato, and Y. Li, "Analysis of frequency characteristics of small-sized wide-band compound transformers," *IEEE Trans. Magn.*, vol. 34, no. 4, pp. 1348–1350, Jul. 1998, doi: 10.1109/20.706544.

[21] *RF Transformer TCM2-33X+*, TCM2-33X+ Datasheet, Mini-Circuits Corp., New York, NY, USA, Oct. 2019.

[22] A. Darwish, S. S. Refaat, H. Abu-Rub, and H. A. Toliyat, "PD signal propagation in GIS: Ultra-high frequency detection-based modeling," *IEEE Sensors J.*, vol. 20, no. 16, pp. 9417–9426, Aug. 2020, doi: 10.1109/JSEN.2020.2988840.

[23] M. Siegel, M. Beltle, S. Tenbohlen, and S. Coenen, "Application of UHF sensors for PD measurement at power transformers," *IEEE Trans. Dielectr. Electr. Insul.*, vol. 24, no. 1, pp. 331–339, Feb. 2017, doi: 10.1109/TDEI.2016.005913.

[24] H. Chai, B. T. Phung, and S. Mitchell, "Application of UHF sensors in power system equipment for partial discharge detection: A review," *Sensors*, vol. 19, no. 5, p. 1029, 2019, doi: 10.3390/s19051029.

[25] X. Ge, H. Ji, X. Cui, and C. Li, "Movement behavior and partial discharge of the single metallic particle in GIS at operated voltage," *IEEE Trans. Plasma Sci.*, vol. 47, no. 9, pp. 4319–4328, Sep. 2019, doi: 10.1109/TPS.2019.2930349.

[26] R. Mishra, H. Muthukrishnan, A. Ramanan, and R. Sarathi, "Understanding partial discharge activity in GIS due to particle movement under high frequency AC voltage adopting UHF technique," in *Proc. 6th Int. Conf. Ind. Inf. Syst.*, Kandy, Sri Lanka, Aug. 2011, pp. 93–97, doi: 10.1109/ICIINFS.2011.6038047.

[27] B. Fruth and L. Niemeyer, "The importance of statistical characteristics of partial discharge data," *IEEE Trans. Electr. Insul.*, vol. 27, no. 1, pp. 60–69, Feb. 1992, doi: 10.1109/14.123441.

[28] R. J. Van Brunt, "Stochastic properties of partial-discharge phenomena," *IEEE Trans. Electr. Insul.*, vol. 26, no. 5, pp. 902–948, Oct. 1991, doi: 10.1109/14.99099.

[29] P. Welch, "The use of fast Fourier transform for the estimation of power spectra: A method based on time averaging over short, modified periodograms," *IEEE Trans. Audio Electroacoustics*, vol. AU-15, no. 2, pp. 70–73, Jun. 1967, doi: 10.1109/TAU.1967.1161901.

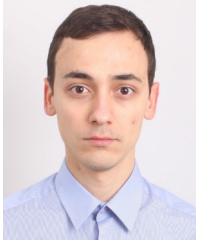

KRISTIAN CHAVDAROV DIMITROV received the B.S. degree in telecommunications engineering (radio communication) from Technical University, Sofia, Bulgaria, in 2015, and the M.S. degree in electrical and electronic engineering from Yonsei University, South Korea, in 2019, where he is currently pursuing the Ph.D. degree in electrical and electronic engineering. His research interests include SAR antenna, waveguide slot, and microstrip patch array antennas.

YONGSHIK LEE (Senior Member, IEEE) was born in Seoul, South Korea. He received the B.S. degree from Yonsei University, Seoul, in 1998, and the M.S. and Ph.D. degrees in electrical engineering from the University of Michigan, Ann Arbor, MI, USA, in 2001 and 2004, respectively. In 2004, he was a Postdoctoral Research Associate at Purdue University, West Lafayette, IN, USA. From 2004 to 2005, he worked as a Research Engineer at EMAG Technologies Inc., Ann Arbor. In 2005, he joined with Yonsei University, where he is currently a Professor. His current research interests include passive and active circuitry for microwave and millimeter-wave applications, electromagnetic metamaterials, and nonradioactive wireless power transfer techniques.

JAE-HO YOUN received the B.S. and M.S. degrees in electrical engineering from Soonchunhyang University, South Korea, in 2000 and 2002, respectively. He is currently working as the Manager with GABO Corporation Ltd. His research interests include microwave component and power system protection.

CHAN-UK PARK received the B.S. degree in electrical engineering from Sungkyunkwan University, South Korea, in 1985. He is currently working as the Director of GABO Corporation Ltd. His research interests include power system protection and substation automation (SA).

SEUNG WON OH received the B.S. degree from the Department of Information and Communications Engineering, MOKPO National Maritime University, in 2017, the M.S. degree in executive MBA from Seoul National University, Seoul, South Korea, in 2020, and the Ph.D. degree from the Department of Technology Policy, Yonsei University, in 2023. He is currently working as the CEO of GABO Corporation Ltd., South Korea. His research interests include digital transformation, smart factory, and big data.

MYOUNG-SOO LEE received the B.S., M.S., and Ph.D. degrees from Hanyang University, South Korea, in 1996, 1999, and 2003, respectively. He is currently working as the Chief Research and Development Center Manager with GABO Corporation Ltd., South Korea. His research interests include power system protection and diagnosis of electric power apparatus.